

Assessing the atomic contribution to the Rashba spin-orbit splitting in surface alloys: Sb/Ag(111)

L. Moreschini,¹ A. Bendounan,² I. Gierz,³ C. R. Ast,³ H. Mirhosseini,⁴ H. Höchst,⁵ K. Kern,³ J. Henk,⁴ A. Ernst,⁴ S. Ostanin,⁴ F. Reinert,⁶ and M. Grioni¹

¹Institut de Physique des Nanostructures, Ecole Polytechnique Fédérale de Lausanne (EPFL), CH-1015 Lausanne, Switzerland

²Experimentelle Physik II, Universität Würzburg Am Hubland, D-97074 Würzburg, Germany and Synchrotron Soleil, L'Orme des Merisiers, Saint-Aubin, BP 48, F-91192 Gif-sur-Yvette Cedex, France

³Max-Planck-Institut für Festkörperforschung, D-70569 Stuttgart, Germany

⁴Max-Planck-Institut für Mikrostrukturphysik, D-06120 Halle (Saale), Germany

⁵Synchrotron Radiation Center, University of Wisconsin, Stoughton, Wisconsin 53589, USA

⁶Experimentelle Physik II, Universität Würzburg Am Hubland, D-97074 Würzburg, Germany and Gemeinschaftslabor für Nanoanalytik, Forschungszentrum Karlsruhe, D-76021 Karlsruhe, Germany

(Received 20 October 2008; published 11 February 2009)

We have studied the electronic structure of the Ag(111) $(\sqrt{3}\times\sqrt{3})R30^\circ$ -Sb surface alloy by angle-resolved photoemission. We find two hybrid surface bands, similar to the isostructural Ag(111)-Bi interface. The spin-orbit coupling induced spin splitting in momentum space, however, is strongly reduced from the Bi case. First-principles and model band calculations correctly reproduce this difference. The present results illustrate the complex interplay of atomic and structural contributions at the origin of the large spin separation in these systems.

DOI: 10.1103/PhysRevB.79.075424

PACS number(s): 73.20.At, 79.60.-i, 71.70.Ej

I. INTRODUCTION

The normal spin degeneracy of the electronic states of nonmagnetic solids is lifted by the spin-orbit (SO) interaction in systems that present a structural inversion asymmetry (SIA). This effect, first discussed for nearly free electrons (NFEs) by Rashba and Bychkov (RB),¹ has been extensively studied in semiconductor heterostructures,² with the prospect of future applications where spins could be manipulated by an electric field. It has been shown by angle-resolved photo-electron spectroscopy (ARPES) that an even larger effect occurs at the Au(111) surface.^{3–5} SO-split bands have later been observed at surfaces and interfaces of *p*,^{6–8} transition,^{9–12} and rare-earth¹³ metals, in disordered Au/Ag alloys¹⁴ and in Au quantum wires.¹⁵ Recently, large SO splittings have been measured by ARPES in single-layer ordered metallic alloys formed by high-*Z* metals (Bi and Pb) at the Ag(111) surface.^{16–18} In Bi/Ag(111), in particular, the wave-vector separation ($2 \cdot k_0$; see below) was found to be 1 order of magnitude larger than in Au(111), and much larger than typical values found in semiconductor heterostructures. It would be desirable to clarify the origin of such unexpectedly large values, both for fundamental reasons and because k_0 is an important figure of merit for possible applications.

The RB model considers two-dimensional (2D) free electrons subject to a surface electrostatic potential V_s whose gradient, the surface electric field, is assumed to be oriented along the surface normal \vec{e}_z . The electron spin couples to the magnetic field appearing in the rest frame of the electron. The free-electron parabola is replaced by a more complex but still isotropic dispersion $E_{\pm}(k) = \frac{\hbar^2 k^2}{2m} \pm \alpha_R k$, where the \pm subscript refers to the two spin states, and the quantization axis is perpendicular to \vec{e}_z and to \vec{k} . The Rashba parameter α_R , which is proportional to ∇V_s , indicates the strength of the coupling. A cut along a generic direction within the plane then yields two parabolic branches shifted away from $\vec{\Gamma}$ by

$k_0 = \frac{\alpha_R m}{\hbar^2}$. This picture is qualitatively consistent with the main experimental features, but quantitatively inaccurate, since typical values of ∇V_s yield band splittings orders of magnitude too small. Modern first-principles calculations^{16,19} achieve impressive quantitative agreement with the experimental data, but provide only limited insight of the physical origin of the splitting.

Since the electric field probed by the electron is strongest near the ion cores, a realistic description of the phenomenon should include atomic aspects. This was first accomplished in a tight-binding model, where the SO splitting depends on the product of the surface-potential gradient times the atomic SO parameter.²⁰ For clean metal surfaces the splitting depends not only on the atomic number *Z*, but also on the orbital character of the surface-state wave function, e.g., on the relative sizes of the *p* and *s* components in an *sp* surface state. It has been proposed that the asymmetry of the wave function near the position of the nuclei resulting from mixing different *l* states might be the single most important factor leading to a SO splitting.²¹ On the other hand, the direct or indirect role of the surface potential is illustrated by the observed dependence on the Miller indices of the surface,⁶ and also on the presence of adsorbates.²²

For surface alloys such as Bi/Ag(111) and Pb/Ag(111), the strength of the atomic SO interaction of both the substrate and the overlayer is clearly important, but is not the only relevant parameter. For instance, the SO coupling induced spin splitting measured for the Bi/Ag(111) alloy ($k_0=0.13$ Å⁻¹) is larger than for both the Ag(111) and Bi(111) surfaces. It is also four times larger than for the Pb/Ag(111) alloy ($k_0=0.03$ Å⁻¹),¹⁸ even if the 6*p* atomic SO parameter ζ_{6p} increases by only 37% between Pb (0.91 eV) and Bi (1.25 eV).²³ The inhomogeneous charge distribution within the alloy yields an in-plane component of the surface-potential gradient which, in the presence of an in-plane SIA, also contributes to the SO splitting. The results of a NFE

model including the SO interaction indeed suggest that this term is crucial to achieve very large values of k_0 .²⁴ Moreover, spin-resolved ARPES measurements on Bi/Ag(111) and Pb/Ag(111) have detected a substantial out-of-plane component of the spin polarization, a telltale consequence of the in-plane gradient.²⁵ Surface corrugation, or equivalently the relaxation of the adsorbate layer, is another key parameter that controls the hybridization with the substrate, and therefore the orbital composition of the surface states.^{16,19} Finally, the electronic states of the alloys are more localized than the noble-metal surface states. As a result, they probe the surface-potential gradient more effectively, and the asymmetry of their wave functions is enhanced with respect to the clean metal counterparts.

Only a few combinations of *p*-metal adsorbates and noble-metal substrates have been studied so far. More experimental information is necessary to develop a comprehensive model of SO splitting in these systems. As a step in this direction we present here ARPES data and band-structure calculations for the Sb/Ag(111) surface alloy. The structural parameters of this interface are very close to those of the well-characterized Bi/Ag and Pb/Ag systems. The Sb adatoms replace every third Ag atom in the topmost layer to form a surface alloy with a $(\sqrt{3} \times \sqrt{3})R30^\circ$ surface superstructure with nominal SbAg₂ stoichiometry, similar to the substitutional PbAg₂ and BiAg₂ surface alloys formed by Pb and Bi at the Ag(111) surface. The alloy layer exhibits a preferential hcp stacking relative to the substrate, although an fcc stacking is also possible.^{26–28} Sb and Bi have the same s^2p^3 electronic configuration, but the atomic SO interaction in the Sb 5p valence states is considerably weaker [$\zeta_{5p}(\text{Sb}) = 0.4$ eV].²³ Therefore Sb/Ag(111) provides an almost ideal opportunity to assess the role of atomic contributions to the SO splitting.

II. METHODS

The SbAg₂ surface alloy was prepared by evaporation of 1/3 of a monolayer of Sb on the hot Ag(111) substrate ($T > 400$ K), followed by an annealing at $T = 600$ K. The crystalline order was checked by low-energy electron diffraction (LEED). ARPES measurements were performed in Würzburg and Stuttgart, utilizing He I ($h\nu = 21.2$ eV) radiation from a high-brightness monochromatized helium lamp, and at the Synchrotron Radiation Center in Madison, Wisconsin. Hemispherical electrostatic analyzers were used to measure ARPES intensity maps over acceptance angles of $\pm 13^\circ$ and $\pm 7^\circ$ in the nondispersing direction. The energy resolution was better than 10 meV, and the angular resolution was 0.3° , corresponding to a wave-vector uncertainty of $\sim 0.01 \text{ \AA}^{-1}$.

For the first-principles calculations we followed the multicode approach which already proved to be effective in reproducing the band structure of the Pb/Ag(111) and Bi/Ag(111) surface alloys.^{16,18} The geometric structure of the surface has been obtained by the Vienna *Ab Initio* Simulation Package (VASP). The surface electronic structure has been computed by our relativistic layer Korringa-Kohn-Rostoker (KKR) code,²⁹ using the optimized geometry as input. Since

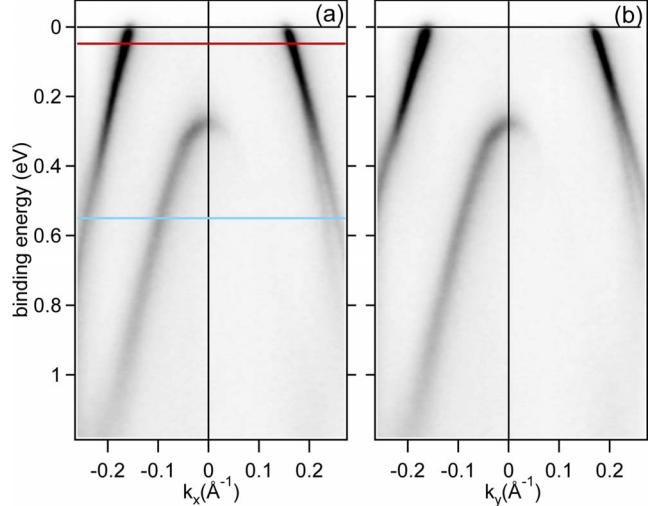


FIG. 1. (Color online) ARPES intensity maps ($h\nu = 21.2$ eV) of the SbAg₂ surface alloy, measured at $T = 100$ K around $\bar{\Gamma}$ along (a) the $\bar{\Gamma}\bar{K}$ and (b) the $\bar{\Gamma}\bar{M}$ directions of the surface BZ.

first-principles calculations do not allow to distinguish *per se* the various contributions (atomic, perpendicular SIA, and in-plane SIA) to the RB splitting, we calculated the surface band structure also within an NFE model. In the latter, the mechanisms involved in the formation of the SO split-band structure are parametrized, thus allowing their interplay to be investigated on a semiquantitative level.

III. RESULTS AND DISCUSSION

Figure 1 shows two ARPES intensity maps for the SbAg₂ alloy, measured around $\bar{\Gamma}$, the center of the hexagonal surface Brillouin zone (BZ), along the $\bar{\Gamma}\bar{K}$ [$\bar{K} = (0.84 \text{ \AA}^{-1}, 0)$] and $\bar{\Gamma}\bar{M}$ [$\bar{M} = (0, 0.72 \text{ \AA}^{-1})$] high-symmetry directions. They show two spectral features dispersing downward from $\bar{\Gamma}$, with an asymmetric intensity distribution that is due to ARPES transition matrix elements and to the geometry of the experiment. Although we will refer hereafter to each of these features as a “band”, both of them exhibit some internal structure, as discussed below. The lower-band maximum is at a binding energy of 0.27 eV and the dispersion is well approximated by a parabolic fit, with effective mass $m^* = -0.15 \pm 0.01 m_e$, where m_e is the bare electron mass. The upper band forms a hole pocket at $\bar{\Gamma}$. It crosses the Fermi level at $k_F(\bar{\Gamma}\bar{K}) = 0.15 \text{ \AA}^{-1}$ and $k_F(\bar{\Gamma}\bar{M}) = 0.17 \text{ \AA}^{-1}$. In this case a parabolic fit would yield ambiguous results because of this slight anisotropy and of the underlying internal structure.

The bands of Fig. 1 appear after the surface alloy is formed. They replace the Ag(111) Shockley state with minimum at ~ 0.06 eV on the clean surface, and reflect the hybridization between the adsorbate and the substrate states. By analogy with the isostructural PbAg₂ and BiAg₂ alloys,^{16,17} we attribute the lower band to states of mainly Sbsp_z and Ags characters. The upper band has mainly p_{xy} character. These assignments are confirmed by our first-principles calculations. However, while in the Bi and Pb alloys each band

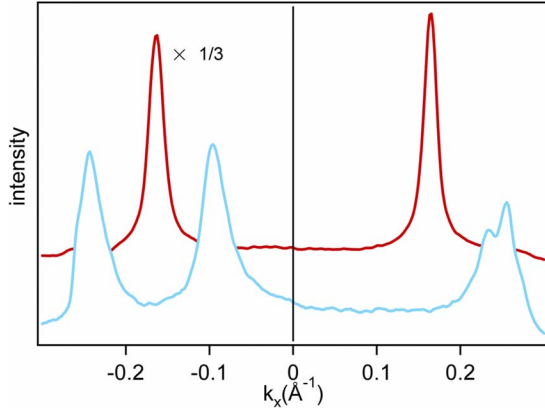


FIG. 2. (Color online) MDCs extracted from the ARPES map of Fig. 1(a), in correspondence of the horizontal lines at $E=0.05$ eV (top, red or dark gray line) and $E=0.55$ eV (bottom, blue or light gray line).

exhibits a clear SO splitting, the effect is considerably smaller here. The two split components are only resolved in the upper band for $k>0.2$ \AA^{-1} , near the edges of the intensity maps. Their different slopes suggest that they cross at about 0.3 eV binding energy and partially overlap up to the Fermi level. Such crossing is at variance with the Bi/Ag and Pb/Ag cases, where the SO-split bands are mainly shifted in k and only cross at the high-symmetry points $\bar{\Gamma}$ and \bar{M} . The lower band does not exhibit a visible splitting, but its trace is broader than the experimental wave-vector uncertainty, suggesting also in this case an underlying structure. The wave-vector broadening can be observed all the way to the band maximum, where the width in the energy direction is small, which again points to the presence of two underlying components.

These qualitative conclusions are confirmed by momentum distribution curves (MDCs) extracted from the intensity map of Fig. 1(a) in correspondence of the horizontal lines at $E=0.05$ eV and $E=0.55$ eV (Fig. 2). At 0.05 eV the line cuts only the upper band, and the corresponding MDC exhibits two sharp peaks on opposite sides of $\bar{\Gamma}$ with nearly Lorentzian line shapes. The MDC at 0.55 eV, which cuts both bands, shows broader line shapes for both bands, and partially resolved split components in the upper band at $k=\pm 0.25$ \AA^{-1} . Remarkably, the intensity at the $k>0$ crossing of the lower band (at $k\approx 0.08$ \AA^{-1}) is totally suppressed.

To get more insight into the cause of the small splitting and of the peculiar crossing in the band structure of Sb/Ag(111), we performed first-principles calculations using the KKR method. The surface relaxation is a crucial parameter, as it influences both the size of in-plane and perpendicular potential gradient, and the amount of hybridization between sp_z and p_{xy} orbitals. The atomic positions as computed using the VASP yielded an outward relaxation of the Sb atoms of about 10%, close to the value of 15% found for Bi in Bi/Ag(111) and consistent with the slightly smaller size of the atomic radius of the Sb atom [2.9 \AA (Sb) vs 3.1 \AA (Bi)]. The value of 10% is somewhat larger than the 2–3 % estimated from independent experiments.^{27,28} On Bi/Ag(111) no experimental structural data are available. However, the

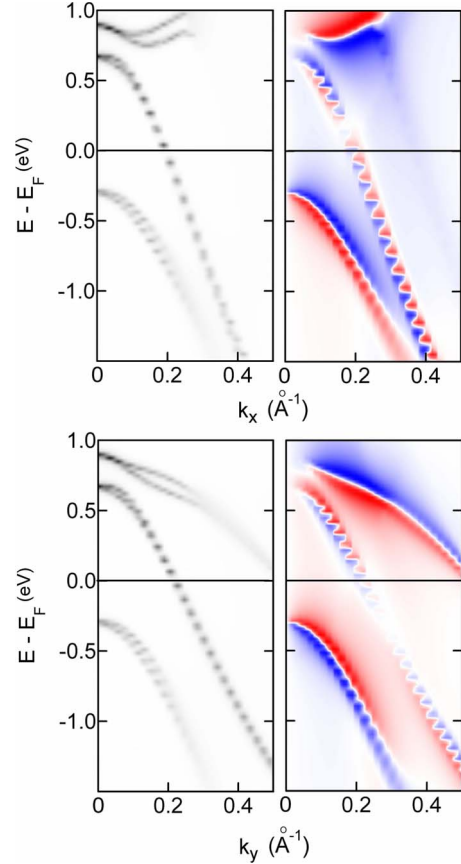


FIG. 3. (Color online) Left: the calculated total spectral density $N=(N_\uparrow+N_\downarrow)$, for the $\bar{\Gamma}K$ (top) and $\bar{\Gamma}M$ (bottom) directions. Right: the in-plane spin polarization P_σ ($\sigma=x,y$ for $k=k_{y,x}$), depicted with positive and negative values represented by blue and red, respectively. White is for zero polarization.

buckling values produced by our simulations seem to indicate that we deal with two very similar interfaces.³⁰

The spectral densities as given by the KKR method are shown in Fig. 3 for the same maps of Fig. 1. The spin polarization of these surface states is mainly in plane and normal to the wave vector. Thus, for the wave vector along the x axis (y axis) the spin is oriented in the y direction (x direction), but with opposite orientation for the spin-split pairs of states. In the calculations we have decomposed the spectral density at a Bi site with respect to the spin components along these directions, thus obtaining the spin-resolved spectral densities N_\uparrow and N_\downarrow . The total spectral density $N=(N_\uparrow+N_\downarrow)$ is shown in the left panels of the figure. The corresponding in-plane spin polarization $P_\sigma=[(N_\uparrow-N_\downarrow)/(N_\uparrow+N_\downarrow)]$ ($\sigma=x,y$ for $k=k_{y,x}$) is shown in the right panels. The dispersion of the calculated bands follows nicely the experimental data. The spin splitting, evident in the right panels, is barely visible in the total density maps. The maximum energy separation (<100 meV) would be detectable with our energy resolution, but the ARPES linewidth in these surface alloys is dominated by surface disorder, which explains why the experiment cannot access this detail. The calculation also reproduces the anomalous crossing in the upper (mainly p_{xy}) band set. It occurs in the vicinity of the Fermi level, in the region showing vanishing spin polarization, i.e., at (E,k_x)

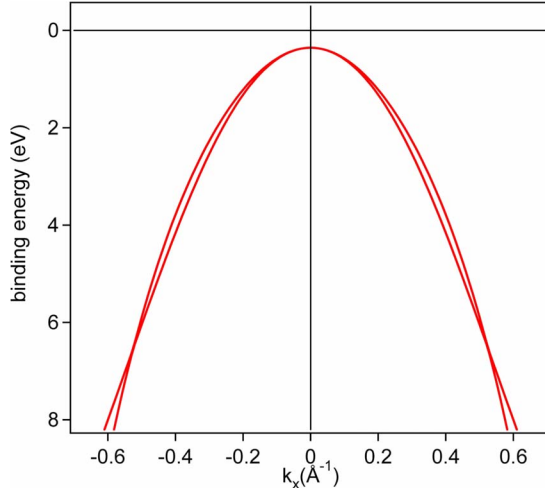


FIG. 4. (Color online) Split bands obtained from an NFE model including the SO interaction.

$= (0.2 \text{ eV}, 0.18 \text{ } \text{\AA}^{-1})$ and $(E, k_y) = (-0.4 \text{ eV}, 0.28 \text{ } \text{\AA}^{-1})$. A third set of bands at higher energies, dispersing upward in the $\bar{\Gamma}K$ direction, is ascribable to p_{xy} ($m_j=3/2$) states.

Interestingly, the outcome of the KKR calculations in terms of orbital hybridization indicates a similar ($\approx 25\%$) admixture of p_{xy} character in the sp_z bands for both the Sb/Ag and the Bi/Ag systems. This is a key point as it shows that the “sensitivity” to the in-plane gradient should be about the same in both systems and cannot explain the difference in the size of the splitting. Therefore, the smaller splitting in Sb/Ag(111) compared to that in Bi/Ag(111) is mainly due to the smaller atomic SO interaction. In other words, a strong in-plane gradient is not effective in generating a strong SO splitting of the interface bands unless supported by a significant atomic contribution from the adsorbate. This consideration is not influenced by the top layer stacking since the calculations show no sizable difference between the faulted and the nonfaulted surface reconstructions.

The individual contributions to the SO splitting cannot be clearly separated, in particular in a first-principles computer code. However, in model calculations that capture the essential ingredients they can be switched on and off individually, and their mutual interplay on the splitting can be analyzed. An NFE model has been recently developed to treat the presence of SIAs in a 2D electron gas.²⁴ It qualitatively illustrates the different contributions from an in-plane and a perpendicular potential gradient to the spin splitting. If we calculate the band dispersion for an in-plane gradient only, we can reproduce the band crossing away from the $\bar{\Gamma}$ point. The result is displayed in Fig. 4 for the $\bar{\Gamma}K$ direction. As the perpendicular gradient is set to zero in this case, there is no momentum offset of the band maximum away from the $\bar{\Gamma}$ point. This can be attributed to the fact that the in-plane gradient results in higher-order contributions than the perpendicular gradient, which shows a linear contribution. Only the combination of the in-plane and the perpendicular gradients will result in a strong enhancement of the spin splitting according to the NFE model. For the present case of Sb/Ag(111) we qualitatively conclude that we have a strong in-

plane contribution of the potential gradient, but since the atomic SO interaction in Sb is much weaker than in Bi, a strong enhancement of the spin splitting cannot be expected. Notice that in a freestanding surface alloy, the in-plane inversion symmetry is conserved, and the SIA comes into play only when considering the interaction with the underlying substrate layers.

From the experimental and theoretical results we can then identify three ingredients to the spin-orbit splitting of the surface states: (i) the atomic contribution, due to the strong Coulomb potential of the nuclei, (ii) the perpendicular potential gradient, due to the surface-potential barrier, and (iii) the in-plane potential gradient, due to the surface geometry. The last one can be viewed as a crystal-field effect of the subsurface layers on the topmost layer. Both the perpendicular and the in-plane gradients break the symmetry of a freestanding Sb/Ag surface layer (which does not show Rashba splitting). The strongest contribution is the atomic one. The other two are orders of magnitude less than the atomic contribution and approximately of the same strength. This hierarchy suggests the following scenario: for a sizable splitting, a strong atomic contribution is inevitable, as can be seen from the surface-state splitting in the series Cu(111)-Ag(111)-Au(111). An additional mechanism (here, the in-plane gradient) can increase the splitting, as seen for Bi/Ag(111) and Pb/Ag(111). However, such mechanism can only “trigger” the effect. Without a strong atomic contribution, the splitting is small, as proven in the present work on Sb/Ag(111).

While the SbAg₂ bands are approximately free-electron-like near the center of the BZ, the dispersion is strongly affected by the lattice potential at larger k values. This aspect is not included in the simple RB model of the SO splitting, and adds interesting structure to the in-plane spin polarization.¹⁶ The departure from an isotropic dispersion is illustrated by the calculated band structure of Fig. 3. Hints of an anisotropy are visible already in the maps of Fig. 1: (i) the Fermi wave vectors of the upper band are different in the two directions, and (ii) the upper and lower bands get closer in energy along $\bar{\Gamma}K$ but not along $\bar{\Gamma}M$. The anisotropy is especially evident in the constant-energy contours of Fig. 5, obtained by cutting the experimental band structure at four binding energies between the Fermi level and 2.1 eV. At E_F [Fig. 5(a)] the map shows a hexagonal contour centered at $\bar{\Gamma}$ from the upper (p_{xy}) band. A second smaller contour, from the lower band, is present in the $E=0.4$ eV map [Fig. 5(b)], but only part of it is visible due to the strong intensity modulation already evident in Fig. 1. Both contours grow in size at larger binding energies. In panel (c) the lower-band contour is also hexagonal, but rotated by 30° with respect to the upper-band contour, which is distorted into a flowerlike shape. Since the highest spin polarization is predicted at the corners of the hexagons,^{16,24} the angular mismatch of the constant-energy contours yields a similar offset in the spin polarization of the two bands. The larger and weaker hexagonal shape, visible in panels (a)-(d) of Fig. 5 and schematically reproduced in Fig. 5(e), is formed from arcs due to the backfolding of the NFE bulk Ag sp conduction band at the BZ boundaries of the surface alloy. These arcs cross the contours of the alloy bands without being distorted. Therefore

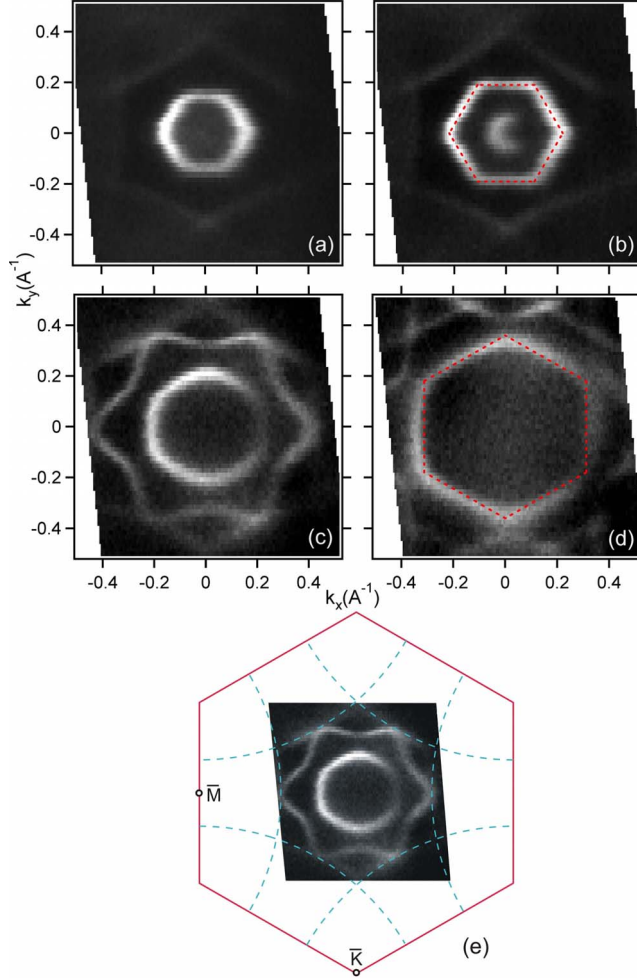


FIG. 5. (Color online) Constant-energy contours obtained at (a) the Fermi level and at (b) 0.4, (c) 1.3, and (d) 2.1 eV binding energies. The dashed hexagons are guides to the eye. Panel (e), which reproduces the data of panel (c), shows the surface BZ and the backfolded contours of the bulk Ag *sp* conduction band.

the backfolding of the Ag bulk band is simply a final-state effect, namely, the diffraction of the outgoing photoelectrons by the ordered overlayer.

It is interesting to compare the hexagonal contours of Fig. 5 with the circular Fermi surfaces of the Shockley states of the clean (111) surfaces of Cu, Ag, or Au. The larger size of the alloy Fermi surface relative to the BZ cannot entirely explain the difference. In particular, for the Au(111) surface the ratio ($k_F/\Gamma M$) is only 30% smaller than the corresponding ratio for the SbAg₂ alloy. The Shockley states of clean noble metals with their weak lattice potential show free-electron-like behavior and thus a circular Fermi surface. The stronger effect of the lattice in the alloy is the result of the more anisotropic ionic charge distribution within the surface plane, where each Sb atom “sees” six Ag nearest neighbors and six Sb next-nearest neighbors with an inequivalent ionic potential. This anisotropy, only partially screened by the valence electrons, is indeed at the origin of the in-plane gradient, which contributes to the SO splitting.

IV. CONCLUSIONS

In summary, we have studied the electronic structure of the SbAg₂ surface alloy. We found obvious similarities with the bands of the isostructural BiAg₂ and PbAg₂ alloys, but a much smaller SO splitting and a non-rigid band shift in wave vector even for k values close to $\bar{\Gamma}$. The experimental data are well reproduced by first-principles relativistic calculations. These results indicate that large in-plane potential gradient, which plays a crucial role in the BiAg₂ surface alloy, is ineffective in producing a large SO splitting unless supported by a strong atomic SO interaction of one of the alloy constituents. On the other hand, the band splitting is not simply proportional to the relevant atomic SO parameter. More data on other surface alloys, grown on different substrates, are necessary to further clarify the interplay of atomic and structural parameters.

ACKNOWLEDGMENTS

M.G. kindly acknowledges clarifying discussions with G. Bihlmayer. This work was supported by the Swiss National Science Foundation and by the MaNEP NCCR. The Synchrotron Radiation Center is funded by the National Science Foundation under Award No. DMR-0537588. A.B. thanks the Alexander von Humboldt Foundation for financial support.

¹Y. A. Bychkov and E. I. Rashba, JETP Lett. **39**, 78 (1984).

²R. Winkler, *Spin-orbit Coupling Effects in Two-dimensional Electron and Hole Systems* (Springer, New York, 2003).

³S. LaShell, B. A. McDougall, and E. Jensen, Phys. Rev. Lett. **77**, 3419 (1996).

⁴G. Nicolay, F. Reinert, S. Hüfner, and P. Blaha, Phys. Rev. B **65**, 033407 (2001).

⁵M. Hoesch, M. Muntwiler, V. N. Petrov, M. Hengsberger, L. Patthey, M. Shi, M. Falub, T. Greber, and J. Osterwalder, Phys. Rev. B **69**, 241401(R) (2004).

⁶Y. M. Koroteev, G. Bihlmayer, J. E. Gayone, E. V. Chulkov, S. Blügel, P. M. Echenique, and P. Hofmann, Phys. Rev. Lett. **93**,

046403 (2004).

⁷K. Sugawara, T. Sato, S. Souma, T. Takahashi, M. Arai, and T. Sasaki, Phys. Rev. Lett. **96**, 046411 (2006).

⁸T. Hirahara, T. Nagao, I. Matsuda, G. Bihlmayer, E. V. Chulkov, Y. M. Koroteev, P. M. Echenique, M. Saito, and S. Hasegawa, Phys. Rev. Lett. **97**, 146803 (2006).

⁹E. Rotenberg, J. W. Chung, and S. D. Kevan, Phys. Rev. Lett. **82**, 4066 (1999).

¹⁰M. Hochstrasser, J. G. Tobin, E. Rotenberg, and S. D. Kevan, Phys. Rev. Lett. **89**, 216802 (2002).

¹¹A. M. Shikin, A. Varykhelov, G. V. Prudnikova, D. Usachev, V. K. Adamchuk, Y. Yamada, J. Riley, and O. Rader, Phys. Rev.

- Lett. **100**, 057601 (2008).
¹²Y. S. Dedkov, M. Fonin, U. Rüdiger, and C. Laubschat, Phys. Rev. Lett. **100**, 107602 (2008).
¹³O. Krupin, G. Bihlmayer, K. Starke, S. Gorovikov, J. E. Prieto, K. Döbrich, S. Blügel, and G. Kaindl, Phys. Rev. B **71**, 201403(R) (2005).
¹⁴H. Cercellier, C. Didiot, Y. Fagot-Revurat, B. Kierren, L. Moreau, D. Malterre, and F. Reinert, Phys. Rev. B **73**, 195413 (2006).
¹⁵I. Barke, F. Zheng, T. K. Rügheimer, and F. J. Himpsel, Phys. Rev. Lett. **97**, 226405 (2006).
¹⁶C. R. Ast, J. Henk, A. Ernst, L. Moreschini, M. C. Falub, D. Pacilé, P. Bruno, K. Kern, and M. Grioni, Phys. Rev. Lett. **98**, 186807 (2007).
¹⁷D. Pacilé, C. R. Ast, M. Papagno, C. Da Silva, L. Moreschini, M. Falub, A. P. Seitsonen, and M. Grioni, Phys. Rev. B **73**, 245429 (2006).
¹⁸C. R. Ast *et al.*, Phys. Rev. B **77**, 081407(R) (2008).
¹⁹G. Bihlmayer, S. Blügel, and E. V. Chulkov, Phys. Rev. B **75**, 195414 (2007).
²⁰L. Petersen and P. Hedegård, Surf. Sci. **459**, 49 (2000).
²¹G. Bihlmayer, Y. M. Koroteev, P. M. Echenique, E. V. Chulkov, and S. Blügel, Surf. Sci. **600**, 3888 (2006).
²²F. Forster, S. Hüfner, and F. Reinert, J. Phys. Chem. B **108**, 14692 (2004).
²³K. Wittel and R. Manne, Theor. Chim. Acta **33**, 347 (1974).
²⁴J. Prempér, M. Trautmann, J. Henk, and P. Bruno, Phys. Rev. B **76**, 073310 (2007).
²⁵F. Meier, H. Dil, J. Lobo-Checa, L. Patthey, and J. Osterwalder, Phys. Rev. B **77**, 165431 (2008).
²⁶S. A. de Vries, W. J. Huisman, P. Goedtkindt, M. J. Zwanenburg, S. L. Bennett, I. K. Robinson, and E. Vlieg, Surf. Sci. **414**, 159 (1998).
²⁷E. A. Soares, C. Bittencourt, V. B. Nascimento, V. E. de Carvalho, C. M. C. de Castilho, C. F. McConville, A. V. de Carvalho, and D. P. Woodruff, Phys. Rev. B **61**, 13983 (2000).
²⁸P. D. Quinn, D. Brown, D. P. Woodruff, P. Bailey, and T. C. Q. Noakes, Surf. Sci. **511**, 43 (2002).
²⁹J. Henk, in *Handbook of Thin Film Materials*, edited by H. S. Nalwa (Academic, San Diego, 2001), Vol. 2, Chap. 10, p. 479.
³⁰Other calculations give a much higher value (0.85 Å) for the Bi relaxation in Bi/Ag(111) (Ref. 19). Nevertheless, the same reference gives a Pb relaxation in Pb/Ag(111) consistently higher than that observed experimentally [J. Dalmas, H. Oughaddou, C. Leandri, J. M. Gay, G. Le Gay, G. Treglia, B. Aufray, O. Bunk, and R. L. Johnson, Phys. Rev. B **72**, 155424 (2005)].